Optimal Sampling Lattices for High-Fidelity CT Reconstruction

Klaus Mueller, *Senior Member, IEEE* and Fang Xu, *Member, IEEE*

***Abstract* – We show that the familiar Cartesian lattice, while convenient for signal processing and representation, is sub-optimal when it comes to signal fidelity. We explore various applications of optimal sampling lattices, such as the Hexagonal and Body Centered Cartesian (BCC) lattices for 3D Computed Tomographic (CT) Reconstruction, both in terms of the (2D) detector and the (3D) reconstructed object. We find that BCC lattices compare favorably with CC lattices for both CT data acquisition and reconstruction. For example they increase the recovery and detectability of small features, such as small tumors in the brain.**

I. INTRODUCTION

The Cartesian lattice, with grid samples distributed on a separable, orthogonal raster of most often equal grid spacing in all dimensions, is very convenient for representation, indexing, and interpolation, and it is also easy to conceptualize. It is mostly for these reasons that the regular Cartesian lattice has become the most dominantly used regular raster structure today. However, recent years have brought an increased awareness with respect to the sub-optimality of the Cartesian grid topology. The key observation motivating this is made in the frequency domain. When assuming a radially symmetric (spherical) frequency spectrum of the rasterized signal, then the optimal packing of the alias spectra is not a Cartesian lattice but a hexagonal one, since such a lattice packs the frequency spectrum spheres closest together [1]. This, by ways of the Fourier scaling theorem, stretches the samples in the co-domain, here the spatial domain, furthest apart, leading to the coarsest possible sampling pattern without risking (pre-) aliasing. This makes possible a reduction of grid points to 87% in 2D, 71% in 3D, and 50% in 4D, with a direct consequence being a reduction in storage by these amounts, which can affect cache behavior as well. But more important for our work, grid processing costs are reduced by these amounts as well, if these costs are strongly related to the number of grid points. This pays off mostly within iterative reconstruction frameworks [4][5], but their use in analytical frameworks has also been studied [2]. For the former, using optimal lattices brings significant savings since iterative algorithms typically project and back-project the evolving reconstruction many times, and thus a reduction in grid complexity can make a considerable difference in running time. Finally, optimal sampling lattices also help make volume visualization more efficient [6][7].

In the current work, we shall look at CT reconstruction and optimal lattices from a different perspective, that is, from the standpoint of lattice isotropy and uniformity. We will show that due to these intrinsic properties, optimal lattices can reconstruct and acquire fine detail significantly better than the standard Cartesian lattices, without a loss of performance. This is important, for example, when it comes to the detection of small lesions in CT. At the same time, optimal lattices can also provide a higher-fidelity sampling of the incoming X-ray signal on the detector plane, to be explored in this paper as well.

Manuscript received November 10, 2009. This work was supported in part by NIH grant R21 EB004099-01.

Klaus Mueller is with the Center for Visual Computing, Computer Science Department at Stony Brook University, NY, USA. (telephone: 631-632-1524, e-mail: mueller@cs.sunysb.edu).

Fang Xu was with is with the Center for Visual Computing, Computer Science Department at Stony Brook University, NY, USA. He is now with Siemens Corporate Research, Princeton, NJ, USA. (email: xufang@gmail.com).

II. THEORY

The 2D hexagonal lattice is depicted in Figure 1a. Its 3D equivalent in terms of space-optimality is the Body Centered Cartesian (BCC) lattice (illustrated in Figure 1b – in all of Figure 1, the grid distances have been expressed in terms of its frequency bandwidth-equivalent Cartesian (CC) lattice). The frequency transform of the hexagonal lattice is another hexagonal lattice. The frequency transform of the BCC lattice is the Face-Centered Cartesian (FCC) lattice, which

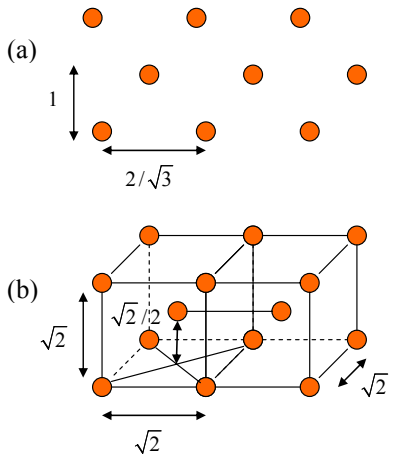

Fig. 1. (a) hexagonal lattice, (b) BCC lattice

has the tightest best sphere packing possible.

In a uniform lattice the maximum spatial distance of an arbitrary sample to a lattice point is independent of direction. Thus, the Voronoi cell of such a uniform lattice must be a sphere. A collection of spheres, however, cannot be space-filling and thus optimal uniformity cannot be achieved in practice. We therefore seek a lattice with a Voronoi cell that is closest to a sphere. The sphere has the smallest surface area enclosing a given volume. Setting the volume of a sphere to unity, the surface area S_s is:

$$S_s = 4\pi(\frac{1}{\sqrt[3]{4/3\cdot\pi}})^2 = 4.83 \quad (1)$$

The surface area S_{cc} of a unit cube is an obvious S_{cc}=6. The Voronoi cell of the BCC lattice is the truncated octrahedron, and the surface area S_{bcc} of its unit cell is:

$$S_{bcc} = (6+12\sqrt{3})\cdot(\frac{1}{\sqrt[3]{8\sqrt{2}}})^2 = 5.31 \quad (2)$$

Here the second term is the lattice parameter value setting for a unit cell. We see that the BCC lattice is about 10% worse than the sphere, but 12% better than the CC lattice. Finally, let us have a look at the Face-Centered Cartesian (FCC) lattice, which is the dual of the BCC lattice. Its Voronoi cell is the rhombic dodecahedron, and the surface area S_{fcc} of its unit cell is:

$$S_{fcc} = 8\sqrt{2}\cdot(\frac{1}{\sqrt[3]{(16/9)\sqrt{3}}})^2 = 5.34 \quad (3)$$

Again, the second term is the lattice parameter value setting for a unit volume cell. Thus, the BCC lattice is slightly more isotropic than the FCC lattice, under this metric. We therefore choose the BCC lattice for the work presented here.

In a parallel-beam configuration, each projection essentially constitutes a radial slice of the object's Fourier spectrum (the *Fourier Slice Theorem*). This Fourier polar grid has a number of important implications with regard to the sampling lattices used in reconstruction and acquisition. Most important for our discussion is that the Fourier Slice Theorem results in the acquisition of a radially symmetric frequency spectrum. Therefore, an optimal sampling lattice, which assumes this type of spectrum (as noted before) is appropriate.

Thus far we have only considered the 2D case, but we aim to reconstruct in 3D. This yields a sphere only in Radon space. In the limit, for parallel-beam projection, the frequency space is a stack of radially symmetric spectra, which only partially fulfills the optimal lattice assumption. We are using cone-beam projections for CT reconstruction, however, which has an arrangement conforming somewhat better to the sphere.

III. IMPLEMENTATION

Detectors are typically composed of an array of square pixels. Novel optical video cameras have recently been introduced which adopt hexagonal lattices for more isotropic sampling. This has led us to explore these types of lattices also for X-ray detection. However, a standard Cartesian grid is more efficient for GPU-accelerated CT reconstruction [8], allowing an easier mapping of the voxels onto the projections. Else, the added overhead incurred by application of fragment shader-bound interpolation filters would cause a significant loss in performance, as this would occur at a complexity of $O(N^4)$, assuming we have $O(N)$ projections to reconstruct N^3 voxels. We therefore resample the acquired projections from the hexagonal grid onto a Cartesian grid before reconstruction begins. This enables fast hardware accelerated bilinear interpolation in a voxel-driven backprojection scheme. It also lowers the complexity of the hex-grid interpolation by an order of magnitude since it is now a pre-processing step.

Our reconstruction framework uses the standard Feldkamp cone-beam reconstruction algorithm, in a GPU-accelerated framework [8]. Essential for the work described here is the fact that the back-projection operations are independent of the underlying lattice, due to the voxel-driven backprojection scheme. The GPU-accelerated reconstruction algorithm itself only requires a slight change for handing the BCC lattice. Since for BCC each slice is a standard Cartesian lattice, we can employ our interpolation fragment program unchanged. The only item requiring change is the vertex program that needs to shift the slice polygon for each odd slice index.

We have chosen to keep the total number of voxels the same. This reduces the in-slice lattice spacing from the space-optimal $\sqrt{2}$ to $\sqrt[3]{2}$ = 1.26 (and an inter-slice distance of $\sqrt[3]{2}/2$), yielding a system where the reconstruction performance in our GPU-accelerated framework does not suffer at all. However, as seen next, this arrangement is able to resolve small features better than the standard lattice with both in-slice and inter-slice spacing of 1.

IV. RESULTS

We explored three detector lattice configurations. We up-sampled these acquired images and compared them with a directly acquired (via simulation) X-ray image at the same grid resolution. All simulation traced multiple (16) rays per pixel to simulate X-ray beams. We explored the following configurations (see Fig. 1):

1. The standard Cartesian case, assuming a lattice spacing of 1, and a (square) detector element area of 1 (blue curve).
2. A standard Cartesian lattice with twice the resolution of #1, which gives a detector element area of 0.25 (yellow curve).
3. The space-optimal (hexagonal) lattice version of #2, with 86% ($\sqrt{3}/2$) of the elements of #2. Here, the detector element area is increased by 23% to 0.28 allowing for better SNR (magenta).

All images were up-sampled to twice the resolution of the second configuration. We used a linear filter for all cases. For the Cartesian grids we used bilinear interpolation, while for the hexagonal grid we employed a filter based on barycentric coordinates. We performed our study using the Marschner-Lobb (ML) dataset [3], which has almost uniform frequency content all the way up to the Nyquist limit (see Figure 2 for an iso-surface volume rendering). Measurements were taken for an angular range of 0-45° at 10° increments, and the projections were compared with the simulated projection obtained at the same angle in a numerical sense, via its RMS error. The results of this study are shown in Fig. 3. We observe that the space-optimal hexagonal detector lattice performs significantly better than the equivalent standard Cartesian lattice, at a greater detector element area. Thus, the hexagonal detector combines the better area efficiency, which has favorable implications with respect to the signal-to-noise ratio, with better sampling fidelity.

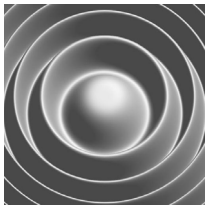

Fig. 2. A volume rendering of the ML function.

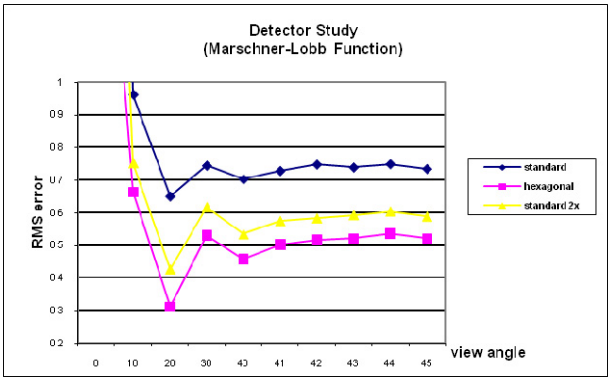

Fig. 3. Projection results for the ML function, for various detector lattice configurations.

We then used the up-sampled detector images for 3D reconstruction. We first reconstructed a dataset of a human toes scan, both onto a standard Cartesian lattice and then on the BCC lattice with the same number of elements, using our streaming CT reconstruction application. Figure 4 shows visualizations from the same viewpoint and at the same iso-surface setting. We used direct volume rendering with a few compositing steps for iso-surface visualization. We notice a slightly better recovery of the features with DVR and an overall smoother surface quality. But the differences are not overly dramatic.

However, the true advantages of optimal lattices lie in their ability to recover small features better, and with less sensitivity to orientation (due to its more isotropic sampling). A common task in medical imaging is the detection of small lesions and tumors. To explore the performance of the two candidate lattices in this context, we generated a 3D phantom dataset consisting of blobs of various sizes and generated (standard Cartesian) projections of these. The projections had a resolution such that the smallest blobs would still be detectable to at least 1-2 pixels. We then reconstructed these blobs on both a CC and the equivalent BCC lattice at a resolution matching that of the projections. At this lattice resolution the size of the smallest blobs amounted to about 1.5 voxels. The reconstruction results are shown in Fig. 5. We see that only the BCC lattice is able to recover the smaller blobs, and overall the blobs appear better refined.

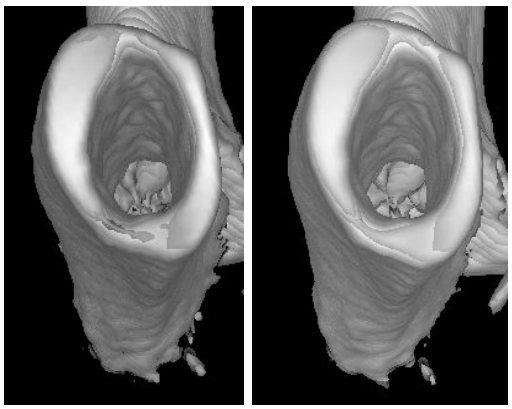

Fig. 4. Iso-surface rendering of a reconstruction of a human toes scan: (left) CC-lattice reconstruction, (right) BCC-lattice reconstruction.

Next, we generated a tumor brain phantom by embedding a selection of randomly distributed small tumors into an existing brain volume dataset. We generated projections and reconstructed them as well, using the same protocol than for the blob phantom. Fig. 6 shows a slice of this reconstruction. Again, we observe that the BCC lattice is able to recover almost all of the tumors, while the CC lattice fails in many cases.

V. CONCLUSIONS

We have demonstrated that BCC lattices compare favorably with CC lattices for CT data acquisition and reconstruction. For reconstruction, we have focused on accuracy only, that is, we have used the same number of lattice points, but distributed them into the more isotropic configuration of the BCC lattice. We found that this results in somewhat minor overall quality improvements, at least for the dataset we have tested, But, more importantly, we have also found that the BCC lattice increases the recovery and detectability of small features, for example, small tumors in the brain. This is an important aspect in CT practice.

We have also investigated the use of optimal lattices on X-ray detectors, and our findings were that the better isotropy of hexagonal lattices enables the detector elements to be made larger, but yet obtain more accurate projections.

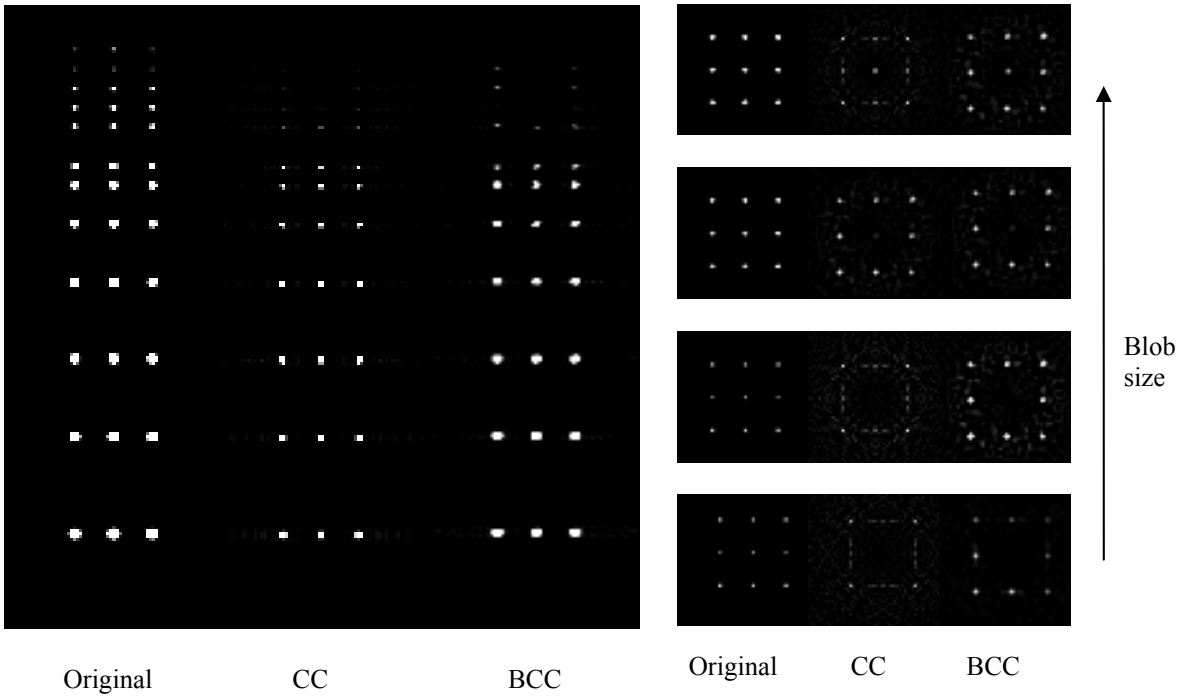

Fig. 5. Blob phantom study. (Left): a row of blobs of decreasing size extends diagonally across space. The projections had a resolution such that the smallest blobs would still be detectable to at least 1-2 pixels. We then reconstructed these blobs on both a CC and the equivalent BCC lattice at a resolution matching that of the projections. At this lattice resolution the size of the smallest blobs amounted to about 1.5 voxels. (Right): The CC and BCC lattice reconstructions of these are shown as cross-sections: first the blob phantom, and next to it its reconstructions. We observe that the BCC lattice recovers the small blobs significantly better, and in some cases is the only lattice to recover them.

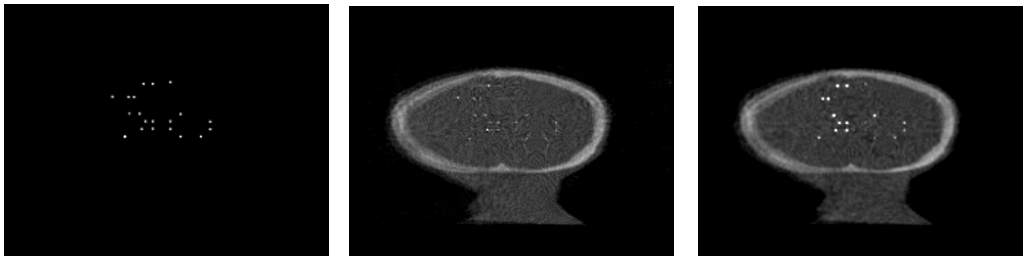

Fig. 6. Tumor phantom study, which is a more realistic experiment than the blob study. A set of small tumors was distributed in 3D (a slice of these is shown on the left) and was embedded into a brain volume dataset. A corresponding slice of the reconstruction results using the CC and the BCC lattices are shown to the right, respectively. We see that the BCC lattice cannot recover all of them either (due to their small size), but it recovers significantly more of them and at higher intensity.

Future work on reconstruction lattices will focus on "smart" multi-resolution grids, which adapt their resolution to the projection images provided. This, in some ways, is a continuation of earlier work [9], where volume rendered images are generated directly from the projections and no volume lattice is ever generated.

Future work on hexagonal detector lattices should also focus on further explorations of the tradeoff in lattice resolution and detector element size. More experiments will help to define the optimal configurations in that respect, given the task of the application. This goes in hand with more research on better interpolation filters for the subsequent hexagonal-Cartesian regridding.

VI. REFERENCES

[1] J. Conway and N. Sloane. *Sphere Packings, Lattices and Groups.* Springer, 3rd edition, 1999.

[2] M. Knaup, S. Steckmann, O. Bockenbach, M. Kachelrieβ, "CT image reconstruction using hexagonal grids," IEEE Nuclear Science Conference, 2007.

[3] S. Marschner, and R. Lobb, "An evaluation of reconstruction filters for volume rendering," *Proc. IEEE Visualization*, pp. 100-107, 1994

[4] S. Matej, R.M. Lewitt, "Efficient 3D grids for image-reconstruction using spherically-symmetrical volume elements," *IEEE Trans. Nuclear Science*. 42:1361-1370, 1995.

[5] K. Mueller, R. Yagel, "The use of dodecahedral grids to improve the efficiency of the Algebraic Reconstruction Technique (ART)," Annals of Biomedical Engineering, p. S-66, 1996.
[6] N. Neophytou, K. Mueller, "Space-time points: 4D Splatting on efficient grids," Symposium on Volume Visualization and Graphics, pp. 97-106, 2002.
[7] T. Theußl, T. Möller, and E. Gröller, "Optimal regular volume sampling," *Proc. I EEE Visualization*, pp. 91–98. 2001.
[8] F. Xu, K. Mueller, "Real-time 3D computed tomographic reconstruction using commodity graphics hardware," *Physics in Medicine & Biology*, 52: 3405-3419, 2007.
[9] F. Xu and K. Mueller, "GPU-Accelerated D^2VR," *Volume Graphics Workshop*, pp. 23-30, 2006.